

Buried topological edge state associated with interface between topological band insulator and Mott insulator

H. Ishida¹ and A. Liebsch²

¹*College of Humanities and Sciences, Nihon University, Tokyo, 156-8550, Japan*

²*Peter Grünberg Institute and Institute of Advanced Simulations,
Forschungszentrum Jülich, 52425 Jülich, Germany*

(Dated: July 17, 2018)

The electronic structure at the interface between a topological band insulator and a Mott insulator is studied within layer dynamical mean field theory. To represent the bulk phases of these systems, we use the generalized Bernevig-Hughes-Zhang model that incorporates the Hubbard-like onsite Coulomb energy U in addition to the spin-orbit coupling term that causes band inversion. The topological and Mott insulating phases are realized by appropriately choosing smaller and larger values of U , respectively. As expected, the interface is found to be metallic because of the localized edge state. When the Coulomb energy in the Mott insulator is close to the critical value, however, this edge state exhibits its largest amplitude deep within the Mott insulator rather than at the interface. This finding corresponds to a new type of proximity effect induced by the neighboring topological band insulator and demonstrates that, as a result of spin-orbit coupling within the Mott insulator, several layers near the interface convert from the Mott insulating phase to a topological insulating phase. Moreover, we argue that the ordinary proximity effect, whereby a Kondo peak is induced in a Mott insulator by neighboring metallic states, is accompanied by an additional reverse proximity effect, by which the Kondo peak gives rise to an enhancement of the density of states in the neighboring metallic layer.

PACS numbers: 73.20.-r, 71.30.+h, 71.27.+a, 71.70.Ej

I. INTRODUCTION

The role of Coulomb correlations in topological band insulators has recently received wide attention.¹ As a result of spin-orbit coupling, the band structure of these materials exhibits charge excitation spectra whose physical characteristics can depend strongly on the Coulomb interaction. Iridium compounds, such as Na_2IrO_3 and $\text{A}_2\text{Ir}_2\text{O}_7$ ($\text{A}=\text{Pr},\text{Eu}$) have recently been proposed as materials in which the interplay of spin-orbit interaction and electronic correlation effects might be important.^{2,3} The phase diagram of a prototype bulk system of this kind was studied by Yoshida *et al.*⁴ within an extension of the two-band model proposed by Bernevig, Hughes, and Zhang (BHZ),⁵ where an onsite Hubbard term is included to account for correlations. It was shown that, in the paramagnetic limit, such a system exhibits a first-order quantum phase transition, where the weakly correlated phase corresponds to a topological band insulator and the strongly correlated phase to a Mott insulator.

At surfaces of topological insulators, metallic edge states may exist which are protected against perturbations associated with impurities and other interactions that do not break the time-reversal symmetry of the system.⁶⁻¹⁰ Because of these unique properties, heterostructures involving topological band insulators¹¹⁻¹⁶ are presently of great interest since they might be relevant for future technological applications. For instance, as shown by Ueda *et al.*,¹⁴ the interface of a topological band insulator and a Mott insulator also exhibits an edge state which maintains its helical characteristics within the Mott insulator. Moreover, the quasi-particle

properties and depth profile of this state within the Mott insulator depend strongly on the local Coulomb energy.

In the present work we study the role of electronic correlations at the interface between a topological insulator and a Mott insulator. The important difference between our approach and the one by Ueda *et al.*¹⁴ is that we include spin-orbit coupling also within the Mott insulator. Thus, with decreasing Coulomb energy, the Mott insulator does not become a metal but a topological band insulator. The electronic properties in the vicinity of the interface are treated self-consistently by using the layer dynamical mean field theory (DMFT).¹⁷⁻²³ Local many-body interactions are evaluated via finite-temperature exact diagonalization (ED).²⁴⁻²⁶ Separate single-site DMFT calculations are performed for the asymptotic semi-infinite bulk regions. Their influence on the interface region is taken into account via complex embedding potentials.²⁷ For simplicity, a square lattice geometry is used, as illustrated in Fig. 1.^{4,14,28} To incorporate spin-orbit interactions, the generalized two-orbital BHZ model is used, which includes the site-dependent Coulomb energy as well as the interorbital hybridization.

The main result of this study is the displacement of the edge state from the interface toward the interior of the Mott insulator when the local Coulomb energy on the corresponding side of the heterostructure is near the critical value for the Mott transition. The edge state is then buried deeply within the Mott insulator so that the boundary between the band and Mott insulating phases no longer coincides with the physical interface of the two constituents of the heterostructure. The origin of this novel proximity effect is the fact that the Mott transition is first order. As a consequence, within the coexis-

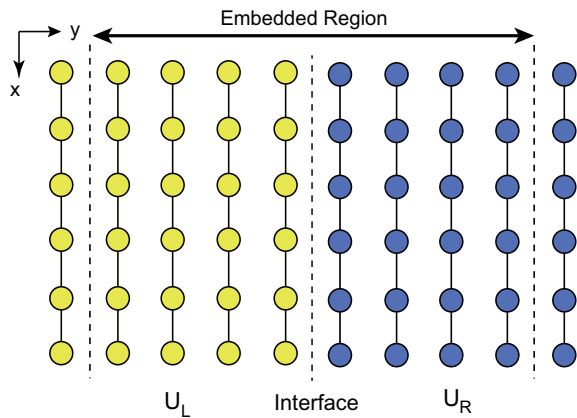


FIG. 1: (Color online) One-dimensional interface between two-dimensional topological band and Mott insulators. The Coulomb energies on the left and right side of the interface are defined as U_L and U_R , respectively. The electronic properties in the embedding region are calculated self-consistently within the layer DMFT. The properties of the asymptotic bulk regions are taken into account via embedding potentials.

tence region topological band and Mott insulating phases compete. Their relative stability depends sensitively on temperature and local Coulomb energy. Moreover, because of the penetration of the edge state wave function into the Mott insulator, near the interface the properties of the nominal Mott insulator are also influenced by the presence of the neighboring topological band insulator. As a result, the Mott insulating phase within a certain depth can be converted into the more stable topological band insulating phase. The edge state is thereby displaced away from the physical interface which becomes the boundary between two weakly and strongly correlated topological band insulators. As the Coulomb energy in the Mott insulator increases beyond the coexistence region, the edge state is localized again at the interface. Its depth within the Mott insulator diminishes as the Mott gap increases. Below the coexistence domain, the edge disappears since the heterostructure then consists of two correlated topological band insulators.

We emphasize that the displacement of the edge state away from the interface of the heterostructure is a consequence of the interorbital hybridization (spin-orbit coupling) in the Mott insulator. In the absence of spin-orbit coupling, the coexistence domain involves trivial metallic and insulating phases so that a topological band insulating solution does not occur. Thus, if an edge state exists, it is localized at the physical interface.

We also demonstrate that the ordinary proximity effect,^{20,22,29,30} i.e., the appearance of a Kondo peak in a Mott insulator due to neighboring metallic states, is accompanied by an secondary reverse proximity effect, as a result of which the Kondo peak leads to an increase of the density of states (DOS) in the neighboring metallic layer.

The outline of this paper is as follows. Section II presents the main aspects of the theoretical approach. In particular, we introduce the generalized BHZ two-band model which provides the basis for the topological band as well as Mott insulating phases. Also, the embedding scheme is described in which the effect of the asymptotic bulk materials on either side of the interface are taken into account via complex local potentials. Finally, the inhomogeneous layer DMFT is outlined, as well as the finite-temperature exact diagonalization scheme for the treatment of local many-body interactions. Section III provides the discussion of the results. We first present the phase diagram of the asymptotic bulk materials and illustrate the edge state at the solid-vacuum interface. The main part discusses the electronic properties of the interface between topological band and Mott insulators, in particular, the location of the edge state as a function of the Coulomb energy within the Mott insulator.

II. THEORY

A. Method

We consider a one-dimensional interface between a two-dimensional (2-D) topological band insulator (BI) and a 2-D Mott insulator (MI), which occupy the left and right half-space, respectively. The x direction is parallel to the interface, while the y axis, which points from left to right, is chosen as the interface normal. To represent the semi-infinite systems on both sides, we employ the generalized Bernevig-Hughes-Zhang model,

$$\begin{aligned} \hat{H} &= \hat{H}_{\text{bhz}} + \hat{H}_{\text{int}} \\ &= (\hat{H}_0 + \hat{H}_{\text{so}}) + \hat{H}_{\text{int}}. \end{aligned} \quad (1)$$

The first term in the second line of Eq. (1),

$$\hat{H}_0 = \sum_{p,\alpha,\sigma} \left(\epsilon_\alpha - \frac{U_y}{2} \right) \hat{n}_{p\alpha\sigma} + \sum_{\langle p,q \rangle, \alpha, \sigma} t_\alpha c_{p\alpha\sigma}^\dagger c_{q\alpha\sigma}, \quad (2)$$

represents two tight-binding bands originating from two orbitals, where $c_{p\alpha\sigma}^\dagger$ ($c_{p\alpha\sigma}$) creates (annihilates) an electron with orbital $\alpha = 1, 2$ in spin state $\sigma = 1$ (\uparrow), -1 (\downarrow) on a 2-D square lattice point at $p = (x, y)$, with x and y giving its x and y positions, respectively. In Eq. (2), ϵ_α and t_α are the site energy and nearest-neighbor hopping integral for orbital α , U_y is the Coulomb energy, which will be described below, $\hat{n}_{p\alpha\sigma} = c_{p\alpha\sigma}^\dagger c_{p\alpha\sigma}$ denotes the orbital occupation, and the summation over p and q in the second term is taken over nearest-neighbor lattice-point pairs. The second term in the second line of Eq. (1), which arises from spin-orbit coupling and is responsible for the opening of a topological energy band gap, reads

$$\hat{H}_{\text{so}} = t_{12} \sum_{\langle p,q \rangle, \sigma} i\sigma \left[e^{i\theta\sigma} c_{p2\sigma}^\dagger c_{q1\sigma} + e^{-i\theta\sigma} c_{p1\sigma}^\dagger c_{q2\sigma} \right], \quad (3)$$

where θ specifies the hopping direction measured relative to the x axis ($\theta = 0$ and $\pi/2$ correspond to the hopping to the positive x and y directions, respectively). The last term in Eq. (1),

$$\hat{H}_{\text{int}} = \sum_{p,\alpha} U_y \hat{n}_{p\alpha\uparrow} \hat{n}_{p\alpha\downarrow}, \quad (4)$$

expresses the onsite Coulomb repulsion between electrons with opposite spin in the same orbital α . We assume that the Coulomb energy can vary with lattice layers, while it is constant within the same layer. It should be noted that the term $-\frac{1}{2}U_y \hat{n}_{p\alpha\sigma}$ in Eq. (2) ensures that the system becomes electron-hole symmetric when chemical potential μ is chosen as $\mu = 0$.

Yoshida *et al.*⁴ studied the effect of strong Coulomb correlations on a topological band insulator by applying single-site DMFT¹⁷ to periodic 2-D bulk systems described by the same generalized BHZ model. It was shown that the system undergoes a quantum phase transition from a topological band insulator to a Mott insulator when one increases the onsite Coulomb energy U , while keeping the system nonmagnetic. As schematically illustrated in Fig. 2, the phase transition is of first order and exhibits hysteresis behavior, i.e., both topological band and Mott insulating solutions are found if U is within the coexistence region $[U_{c1}, U_{c2}]$. The width of this region decreases with increasing temperature T and vanishes at a critical value T_c .

In the present work, both the topological band insulator on the left half-space and the Mott insulator on the right half-space are represented by the generalized BHZ model as described above. As indicated in Fig. 1, the layer dependent Coulomb energy, U_y , is set to be U_L and U_R in the left and right half-spaces, respectively, where $U_L < U_{c2}$ and $U_R > U_{c1}$ (see Fig. 2 below). We note that our model differs from that in the recent work of Ueda *et al.*¹⁴, in which the Mott insulator was represented by two independent Hubbard bands without the spin-orbit coupling term defined in Eq. (3).

B. Embedding potential

We calculate the finite-temperature Green's function of the interface between two semi-infinite systems by using the layer DMFT technique.¹⁸ A finite number of lattice layers in the interface region is treated explicitly, whereas the effect of the outer regions is taken into account via the embedding potentials²⁷ which include correlation effects in the bulk region.²² As we consider nonmagnetic solutions in the present work, the Green's function and other quantities are diagonal with respect to spin. In the following, we show only the up-spin component of the equations and omit spin indices for simplicity.

By introducing the wave number in the x direction, k_x ,

the Green's function in the embedded region is given as

$$G_{p\alpha,p'\alpha'}(i\omega_n) = \int_{-\pi}^{\pi} \frac{dk_x}{2\pi} e^{ik_x(x-x')} \times \langle y\alpha | [i\omega_n + \mu - \hat{H}_{\text{emb}}(k_x, i\omega_n)]^{-1} | y'\alpha' \rangle, \quad (5)$$

where the embedding Hamiltonian in the mixed representation, \hat{H}_{emb} , is a $2N \times 2N$ matrix with N being the number of the embedded lattice layers. It consists of four terms:

$$\hat{H}_{\text{emb}}(k_x, i\omega_n) = \hat{H}_{\text{bhz}}^N(k_x) + \hat{\Sigma}(i\omega_n) + \hat{s}^L(k_x, i\omega_n) + \hat{s}^R(k_x, i\omega_n), \quad (6)$$

where $\hat{H}_{\text{bhz}}^N(k_x)$ denotes the one-electron part of the Hamiltonian in Eq. (1). The superscript N emphasizes the fact that \hat{H}_{bhz}^N is a $2N \times 2N$ matrix for an isolated slab. The second term in Eq. (6) is the Coulomb self-energy. Within single-site DMFT, it is layer diagonal and k_x -independent:

$$\langle y\alpha | \hat{\Sigma} | y'\alpha' \rangle = \Sigma_{\alpha\alpha'}(y, i\omega_n) \delta_{y,y'}. \quad (7)$$

The last two terms in Eq. (6) are the embedding potentials. Since \hat{H}_{bhz} in Eq. (1) includes only nearest-neighbor hopping terms, \hat{s}^L (\hat{s}^R) is non-vanishing only when both layer indices are equal to y_L (y_R), the outermost layer of the embedded slab region on the left (right) hand side. Thus, they are written as

$$\langle y\alpha | \hat{s}^L | y'\alpha' \rangle = s_{\alpha\alpha'}^L(k_x, i\omega_n) \delta_{y,y_L} \delta_{y',y_L}, \quad (8)$$

$$\langle y\alpha | \hat{s}^R | y'\alpha' \rangle = s_{\alpha\alpha'}^R(k_x, i\omega_n) \delta_{y,y_R} \delta_{y',y_R}. \quad (9)$$

We now explain how we can derive the embedding potential for the left-hand side. We assume that the electronic structure in the half-space to the left of the embedded slab region converges to that of the bulk crystal with Coulomb repulsion energy U_L . Thus, within the single-site approximation, the Coulomb self-energy of all layers is assumed to be identical to that in the interior of the bulk with U_L , $\hat{\Sigma}_L(i\omega_n)$. This quantity is a 2×2 matrix in orbital space. Now, let us consider the Green's function of the semi-infinite solid in which the self-energies of all layers are equal to $\hat{\Sigma}_L(i\omega_n)$. We extract from this Green's function a 2×2 matrix spanned by the two orbital components of the outermost surface layer, which is denoted by $g_{\alpha\alpha'}^L(k_x, i\omega_n)$. The embedding potential, i.e., the 2×2 matrix appearing on the right hand side of Eq. (8), is then given by²²

$$\hat{s}^L(k_x, i\omega_n) = \hat{t}_+ \hat{g}^L(k_x, i\omega_n) \hat{t}_-, \quad (10)$$

with

$$\hat{t}_+ = \begin{pmatrix} t_1 & t_{12} \\ -t_{12} & t_2 \end{pmatrix}, \quad \hat{t}_- = \begin{pmatrix} t_1 & -t_{12} \\ t_{12} & t_2 \end{pmatrix}, \quad (11)$$

where t_+ (t_-) is the transfer matrix for electrons which hop between two nearest-neighbor lattice layers toward the positive (negative) y direction.

In order to obtain \hat{g}^L in Eq. (10), we use the following trick. We add one additional lattice layer having the bulk self-energy $\hat{\Sigma}_L$ on top of the semi-infinite substrate expressed by the embedding potential \hat{s}^L . Then, the 2×2 surface Green's function of the resultant new semi-infinite solid is given by

$$\hat{g}^L = \left[i\omega_n + \mu - \hat{H}_{\text{bhz}}^{N=1}(k_x) - \hat{\Sigma}_L(i\omega_n) - \hat{s}^L \right]^{-1}, \quad (12)$$

where $\hat{H}_{\text{bhz}}^{N=1}(k_x)$ is given by

$$\hat{H}_{\text{bhz}}^{N=1}(k_x) = \begin{pmatrix} \epsilon_1 - \frac{U_L}{2} + 2t_1 \cos k_x & 2t_{12} \sin k_x \\ 2t_{12} \sin k_x & \epsilon_2 - \frac{U_L}{2} + 2t_2 \cos k_x \end{pmatrix}. \quad (13)$$

We now make use of the fact that the semi-infinite solid obtained by putting one bulk lattice on top of the semi-infinite bulk system is exactly the same as that without the additional lattice layer. Thus, \hat{g}^L on the right-hand side of Eq. (10) must coincide with \hat{g}^L calculated by Eq. (12). Thus, by inserting \hat{g}^L in Eq. (12) into the right-hand side of Eq. (10), one obtains a set of equations to determine the three independent elements of the embedding potential, $s_{\alpha\alpha'}^L$, for given k_x and ω_n . In contrast to one-band models, for which one can derive an analytical expression of the embedding potential from a quadratic equation obtained by following the same procedure as described above,²² the embedding potential for the present two-band model can be computed only numerically. To determine \hat{s}^L , one needs the bulk self-energy $\Sigma_L(i\omega_n)$ in Eq. (12), which can be determined from an independent DMFT calculation for the 2-D bulk system with Coulomb repulsion energy U_L , before evaluating the interface properties.

Similarly, the embedding potential for the right-hand side can be derived by combining the two following equations.

$$\hat{s}^R(k_x, i\omega_n) = \hat{t}_- \hat{g}^R(k_x, i\omega_n) \hat{t}_+, \quad (14)$$

$$\hat{g}^R = \left[i\omega_n + \mu - \hat{H}_{\text{bhz}}^{N=1}(k_x) - \hat{\Sigma}_R(i\omega_n) - \hat{s}^R \right]^{-1}, \quad (15)$$

where $\Sigma_R(i\omega_n)$ denotes the Coulomb self-energy of the 2-D bulk system with Coulomb interaction U_R .

C. DMFT equation and exact diagonalization

Starting from some initial self-energy matrix, one calculates the local components of the lattice Green's function for each layer, $g_{\alpha\alpha'}(y, i\omega_n) = G_{p\alpha, p\alpha'}(i\omega_n)$, by using Eq. (5). Then, the bath Green's function determining the Weiss mean-field of layer y is obtained by removing the local self-energy:

$$\hat{g}^0(y, i\omega_n) = \left[\hat{g}^{-1}(y, i\omega_n) + \hat{\Sigma}(y, i\omega_n) \right]^{-1}, \quad (16)$$

where $\hat{\Sigma}(y, i\omega_n)$ is the 2×2 matrix defined by Eq. (7).

In the present work, the quantum impurity problem is solved by making use of the exact diagonalization (ED) formalism,²⁴⁻²⁶ in which $\hat{g}^0(y, i\omega_n)$ is approximated by a noninteracting Green's function of a finite cluster consisting of two impurity levels with energy E_α coupled to n_b bath orbitals with energy ϵ_k . Thus,

$$\hat{g}^0(y, i\omega_n) \approx \hat{g}^{\text{cl},0}(y, i\omega_n) = \left[i\omega_n + \mu - \hat{h}^{\text{cl}}(i\omega_n) \right]^{-1}, \quad (17)$$

with

$$\hat{h}_{\alpha\alpha'}^{\text{cl}}(i\omega_n) = E_\alpha \delta_{\alpha\alpha'} + \sum_{k=1}^{n_b} \frac{v_{\alpha k} v_{k\alpha'}}{i\omega_n - \epsilon_k}, \quad (18)$$

where E_α , ϵ_k and $v_{\alpha k}$ are real fitting parameters chosen such that the weighted sum of $|\hat{g}^0 - \hat{g}^{\text{cl},0}|^2$ over a sufficiently large Matsubara frequency range is minimized.²⁶ Then, after adding the onsite Coulomb repulsion terms Eq. (4) to this $(2 + n_b)$ -level cluster, the interacting Green's function of the cluster, $\hat{g}^{\text{cl}}(y, i\omega_n)$, is derived by combining the Arnoldi algorithm for computing the lowest eigenstates with the Lanczos procedure for calculating the Green's function.²⁵ Finally, the cluster self-energy is obtained from the equation:

$$\hat{\Sigma}^{\text{cl}}(y, i\omega_n) = \left[\hat{g}^{\text{cl},0}(y, i\omega_n) \right]^{-1} - \left[\hat{g}^{\text{cl}}(y, i\omega_n) \right]^{-1}. \quad (19)$$

In the ED formalism, the cluster self-energy is assumed to be a physically reasonable representation of the lattice self-energy. Thus, $\hat{\Sigma}^{\text{cl}}(y, i\omega_n)$ is used as the input self-energy $\hat{\Sigma}(y, i\omega_n)$ in Eq. (5) for the next DMFT iteration. This procedure is iterated until the difference between the input and output self-energy matrices for all the lattice layers in the embedded region becomes sufficiently small. In the calculation presented in the next section, we use $n_b = 8$ bath orbitals (4 per orbital), so that the total number of energy levels per cluster equals 10.

III. RESULTS AND DISCUSSION

In the present work, the parameters of the noninteracting part of the Hamiltonian are chosen as $\epsilon_1 = -1$, $t_1 = -1$, $\epsilon_2 = 1$, $t_2 = 1$, and $t_{12} = 0.5$. The same parameter set was used previously in Ref. 4. We consider only the electron-hole symmetric case with chemical potential $\mu = 0$. In the absence of correlations, the bulk bands extend from -3 to $+3$ and the band gap from -1 to $+1$. The DMFT calculations are performed at a relatively small temperature: $T = 1/\beta = 0.01$.

A. Bulk phase diagram

Figure 2 illustrates schematically the bulk phase diagram of the constituents of the present heterostructure. At small U , one has a weakly correlated topological band

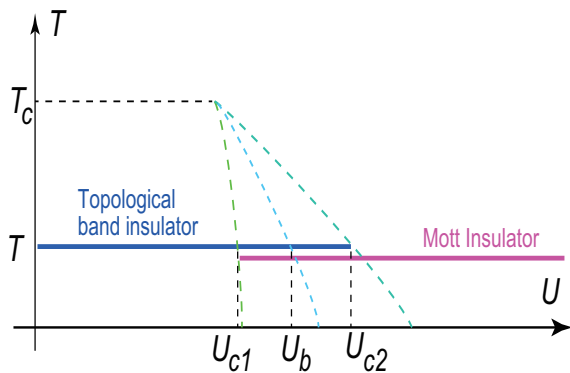


FIG. 2: (Color online) Schematic bulk phase diagram of correlated topological band insulator, derived within generalized BHZ two-orbital model and single-site DMFT. In the region limited by the lines $U_{c1}(T)$ and $U_{c2}(T)$, band and Mott insulating states may coexist. The true phase boundary defining the relative stability of these phases is indicated by the line $U_b(T)$.

insulator which corresponds to the system on the left-hand side in Fig. 1. At large U , the system becomes a Mott insulator which is taken to be the dominant phase on the right-hand side of the interface. We note that in the present model the Mott insulating phase is non-topological with a vanishing Chern number, in contrast to the topological Kondo insulator.^{31,32} The band gap in the band insulator also varies with U . It is largest in the noninteracting limit and gradually decreases with increasing U until U approaches $U_{c2}(T)$. This behavior corresponds to the usual band-narrowing effect, which has been discussed in previous work.^{33,34} As a result of local Coulomb interactions, spectral weight within the region of the bulk bands is transferred to low energies and Hubbard bands appear at high energies. For the parameters specified above, we find that the coexistence region is limited by the boundaries $U_{c1} \approx 11.4$ and $U_{c2} \approx 13.3$. Because of the first-order nature of the Mott transition, various quantities, such as the orbital polarization, the double occupancy of the subbands, the spectral weight at the chemical potential, etc. exhibit the usual hysteresis behavior (not shown here). An important aspect of the interface properties discussed in subsection IIID is the fact that they may be used to determine the relative stability of the band and Mott insulating phases in the coexistence region. For instance, at $T = 0.01$ we estimate $U_b \approx 13.0$.

As will be shown below, an edge state appears at the interface of a weakly correlated topological band insulator and a strongly correlated Mott insulator. The intriguing question then arises what happens to the edge state when the Coulomb energy in the Mott insulator lies within the coexistence region. Depending on the precise values of U and T , the Mott insulating phase can become unstable and may therefore be converted into a band in-

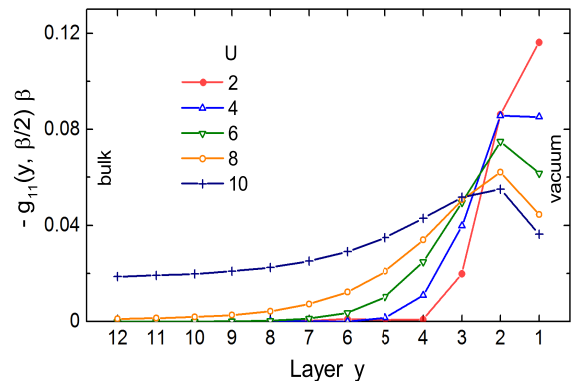


FIG. 3: (Color online) Variation of edge state at bare surface of correlated topological band insulator as a function layer index y for various Coulomb energies U , as calculated within inhomogeneous DMFT. Plotted is the function $-\beta g_{11}(y, \beta/2)$, defined in Eq. (20), which represents the partially integrated density of states within a few T of the chemical potential ($T = 0.01$). The embedding region at the surface comprises 12 atomic layers beyond which bulk behavior is assumed.

ulating phase. Before we discuss this case, we consider in the following two subsections (i) the behavior of the edge state at the bare surface of a topological band insulator and (ii) the properties of the interface between two topological insulators. These results serve a useful reference for the subsequent analysis of the interface with a Mott insulator

B. Edge State at Solid-Vacuum Interface

Figure 3 shows the spectral weight near the chemical potential at the surface of a correlated topological band insulator as a function of distance from the surface for several values of U . Plotted is the function $-\beta g_{11}(y, \beta/2)$ which provides a measure of the DOS within a few T of the chemical potential. This quantity is defined as

$$\begin{aligned} -\beta g_{\alpha\alpha}(y, \beta/2) &= -\sum_n g_{\alpha\alpha}(y, i\omega_n) e^{-i\omega_n\beta/2} \\ &= \pi \int_{-\infty}^{\infty} d\omega F(\omega) N_{\alpha}(\omega), \end{aligned} \quad (20)$$

where $N_{\alpha}(\omega) = -\frac{1}{\pi} \text{Im} g_{\alpha\alpha}(y, \omega + i\delta)$ is the interacting DOS of subband α and the weight function F is defined as: $F(\omega) = 1/[2\pi T \cosh(\omega/(2T))]$. (The width of F is about $5.3T$; its integrated weight is unity.) As a result of particle-hole symmetry, $g_{11}(y, \beta/2) = g_{22}(y, \beta/2)$.

At the surface of a topological insulator, a metallic edge state connecting the bulk valence and conduction bands appears. As the chemical potential is located at the middle of the energy gap when the system is electron-hole symmetric, the edge state contributes to an increase in DOS at μ for several surface layers, which is clearly seen in Fig. 3. With increasing values of U , the gap in the

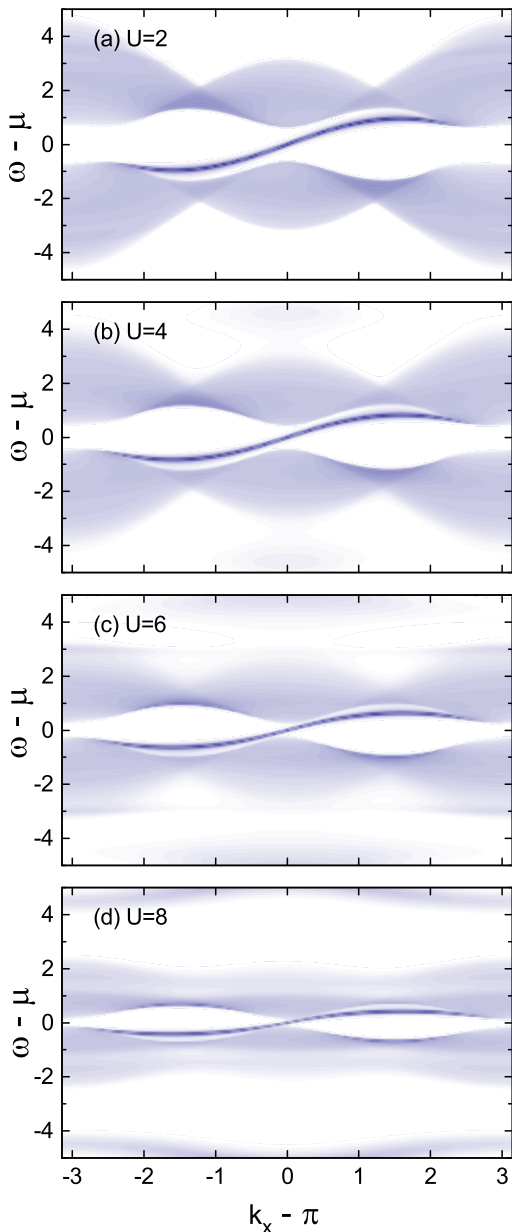


FIG. 4: (Color online) Intensity plot of interacting DOS of orbital $\alpha = 1$, $\sigma = 1$ in surface layer of semi-infinite topological insulator as a function of parallel momentum k_x for several values of U .

topological band insulator diminishes due to correlation effects, so that the penetration depth of the edge state increases. The peak of the edge state at larger U also shifts to the second layer (see below). At the same time, the high-energy tails of $F(\omega)$ on both sides of $\omega = 0$ start overlapping with the bulk bands due to band-gap narrowing. For $U > 8$, this results in a rapid increase in the calculated values of $-\beta g_{11}(y, \beta/2)$ in the interior of the solid.

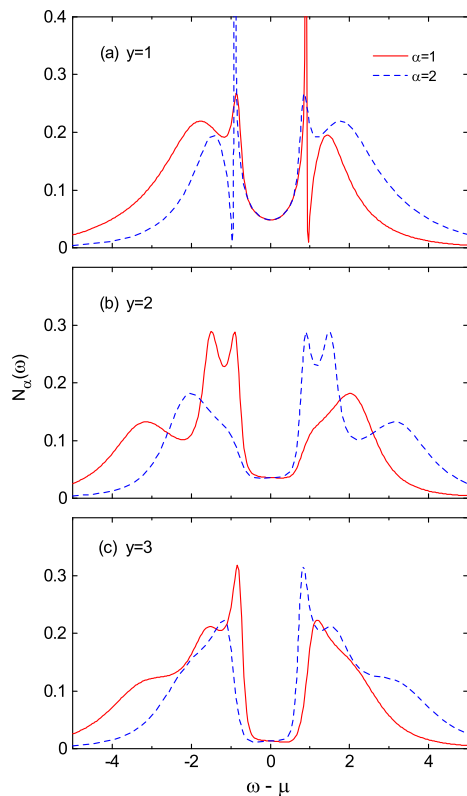


FIG. 5: (Color online) Interacting DOS, $N_\alpha(\omega)$, in first three surface layers of topological insulator at $U = 2$. Solid (red) curves: orbital $\alpha = 1$, dashed (blue) curves: $\alpha = 2$. These spectra are derived by extrapolating the lattice Green's function from Matsubara frequencies to $\omega + i\gamma$ with a small imaginary energy $\gamma = 0.05$ via the routine *ratint*. The spectral weight near $\mu = 0$ in panel (a) is due to the metallic edge state, while the DOS in panel (c) approaches the one characteristic of the bulk band gap.

To illustrate the energy dispersion of the edge state with k_x in the case of a free surface, we show in Fig. 4 the k_x -resolved DOS of the first layer ($y = 1$) for various Coulomb energies. These results were derived by extrapolating the self-energy from the Matsubara axis to real energies via the routine *ratint* (for details see Ref. 26) and then evaluating the integrand on the right hand side of Eq. (5). One can clearly see a metallic edge state crossing the chemical potential $\mu = 0$ at $k_x = \pi$ with a positive group velocity. This indicates that the increase in DOS seen in Fig. 3 for surface layers arises from the edge state around $k_x = \pi$. The energy dispersion curve of the edge state for the down-spin (not shown) is obtained by reflecting the one for the up-spin shown in Fig. 4 with respect to $k_x = \pi$, so that the two dispersion curves with the opposite spins cross at $k_x = \pi$.

With increasing U , the dispersion of the edge state becomes flatter and the bulk band gap is reduced. Also, the width of the bulk bands decreases and Hubbard bands appear below and above the band region. Since

the weight function $F(\omega)$ in Eq. (20) acts nearly like a δ -function at low T , the correlation induced band narrowing of the edge state gives rise to an increase of $-\beta g_{11}(y, \beta/2)$. As shown in Fig. 3, this is indeed the case for layers $y > 2$. Remarkably, this increase of density for $y > 2$ is compensated by a corresponding decrease for layers $y = 1$ and 2, so that the layer-integrated weight of the edge state close to μ remains nearly constant.

According to the dispersions shown in Fig. 4, the DOS of the edge state in the surface layer has the typical shape of a one-dimensional tight-binding system, with a minimum at the center and logarithmic van Hove singularities at the band limits. This is illustrated in Fig. 5(a) for $U = 2$. Panels (b) and (c) indicate how this one-dimensional metallic spectral distribution converts to the one of the topological band insulator as one moves away from the surface. We also note that the DOS at $\omega = \mu$ in Fig. 5 decays with increasing y more slowly than $-\beta g_{11}(y, \beta/2)$ in Fig. 3 owing to a small imaginary energy $\gamma = 0.05$ introduced in extrapolating the lattice Green's function. The peaks at larger energies are sensitive to details of the extrapolation procedure.

As will be seen in Subsection IIID, the low-energy spectral distribution of the edge state of the bare surface shown in Fig. 5 differs qualitatively from the one of edge state at the interface between a topological band insulator and a Mott insulator. The main reason is the appearance of a Kondo peak in the Mott insulator and a new single-particle feature at μ at the surface of the topological insulator.

C. Interface between Topological Band Insulators

Figure 6(a) shows the partially integrated DOS $-\beta g_{11}(y, \beta/2)$ at the interface between a weakly correlated topological band insulator ($U_L = 2$) and more strongly correlated ones ($U_R = 6 \dots 12$) as a function of layer index y . These curves vary monotonously across the interface between two asymptotic values of $-\beta g_{11}(y, \beta/2)$ which are the same as those in the interior of the semi-infinite solid shown in Fig. 3. As mentioned above, the asymptotic values starts growing due to band narrowing only for $U > 8$. Therefore, the curves for $U = 6$ and 8 in Fig. 6(a) are practically constant throughout the system, while the curves for $U = 10$ and 12 exhibit a smooth variation between the two asymptotic values. Evidently, there is no sign of a topological edge state at the interface.

Figure 6(b) shows the occupancy n_1 as a function of layer index y for the three systems shown in panel (a). As we consider electron-hole symmetric systems, the occupancies of the two orbitals are related by $n_2 = 1 - n_1$. It is seen that the orbital polarization, i.e., $n_1 - n_2$, is strongly reduced in the right-hand system with increasing values of Coulomb energy U . (At the Mott transition, both orbitals become half-filled, i.e., $n_1 = n_2 = 0.5$.) Whereas the variation of n_1 occurs very rapidly within one or two

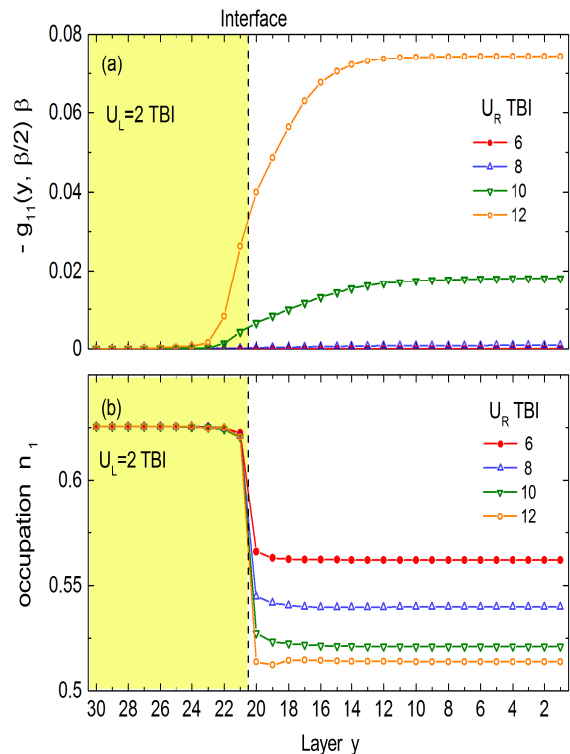


FIG. 6: (Color online) (a) Partially integrated spectral weight, $-\beta g_{11}(y, \beta/2)$, and (b) occupancy n_1 of orbital $\alpha = 1$ as functions of layer index near the interface between two correlated topological band insulators. The systems on the left and right sides have local Coulomb energies $U_L = 2$ and $U_R = 6 \dots 12$, respectively. The location of the interface is indicated by the dashed line. The embedding region consists of 10 layers on the left and 20 layers on the right side of the interface. The asymptotic behavior is derived from DMFT calculations for the respective bulk materials.

layers near the interface, the variation of $-\beta g_{11}(y, \beta/2)$ for $U_R > 8$ is more gradual and comparable to the one at the bare surface shown in Fig. 3. This difference is related to the fact that, because of the finite width of the weight function $F(\omega)$, $g_{11}(y, \beta/2)$ is mainly sensitive to the density of states of the low-energy bulk bands, in particular, at larger U , when the band gap shrinks.

D. Interface between Topological Band and Mott Insulators

We now discuss in more detail the properties of the edge state between a topological band insulator ($U_L = 2$) and a Mott insulator whose Coulomb energy is close to the coexistence region. To obtain the self-consistent solution of the layer-coupled DMFT equation, we adopt the following procedure: On the left (right) boundary of the embedded region, we apply the embedding potential for a semi-infinite solid in the topological insulator phase with

$U_L = 2$ (Mott insulator phase with varying value of U_R), so that the physical states in the asymptotic regions are fixed. Within the embedded region, the initial values of the cluster parameters in Eq. (18), which determine the initial Weiss mean-field for each layer, are taken to be the parameters representing the bulk topological insulator with U_L (Mott insulator with U_R) to the left (right) of the interface boundary. Thus, roughly speaking, initially the system to the left (right) of the boundary surface is in the topological insulator (Mott insulator) phase. We then proceed with the standard DMFT iteration procedure, in which the self-energy and the cluster parameters of the layers in the embedded region are updated according to the prescription described in Sec. II. The iteration procedure is repeated until the local self-energy and Green's function of each layer converge and no longer change with further iterations.

Figure 7(a) shows the partially integrated DOS $-\beta g_{11}(y, \beta/2)$ at $\mu = 0$ for several values of U_R as a function of layer index y . This quantity exhibits a prominent maximum near the interface which is associated with the edge state appearing at the phase boundary between the topological and Mott insulators. The edge state for $U_R = 15$ is seen to be well localized at the interface. The Mott gap in the right-hand system at this Coulomb energy is rather large, so that the edge state decays rapidly into the Mott insulator. In the band insulating system on the left side, the gap is also large, so that the shape of the edge state in this region is similar to the one at the insulator-vacuum interface shown in Fig. 3.

We point out that the amplitude of $-\beta g_{11}(y, \beta/2)$ in the first layer of the Mott insulator for $U_R = 15$ is significantly larger than in the surface layer of the topological band insulator. This enhancement is related to the fact that, as a result of a proximity effect, a Kondo resonance appears in the Mott insulator due to the screening of the localized spins via the helical edge states.¹⁴ Thus, the interface may be viewed as a Kondo-lattice, where the metallicity is associated with the edge state induced by the topological band insulator. This is illustrated in Fig. 8, which shows the variation of the interacting DOS with layer index for $U_L = 2$, $U_R = 15$. In the first layer of the Mott insulator (panel (b)), the DOS at low energies has a three-peak structure, consisting of Kondo peak and van-Hove singularities at the limits of the edge state. The maximum of $-\beta g_{11}(y, \beta/2) \approx 0.33$ at $y = 15$ (see Fig. 7(a)) can therefore serve as a signature of the Kondo peak. In the second layer, only a weak remnant of this peak is observed. In contrast, the first layer of the band insulator is dominated by the van Hove features of the one-dimensional metallic edge state. The deeper layers reveal the appearance of the bulk band gap, in close correspondence to the behavior at the bare surface shown in Fig. 5.

As can be seen in Fig. 8(c), the DOS near $\omega = \mu$ in the surface layer of the topological insulator is enhanced due to the presence of the Mott insulator. This is also evident by comparing $-\beta g_{11}(y, \beta/2) \approx 0.12$ for $U = 2$

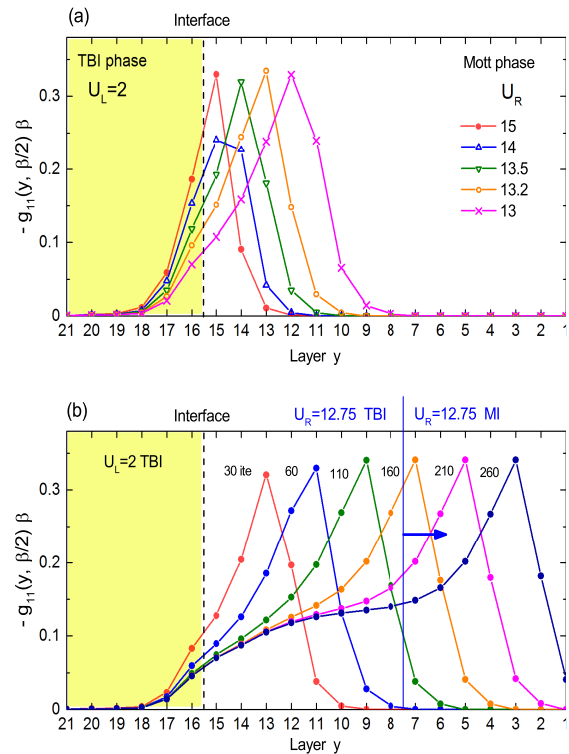


FIG. 7: (Color online) (a) Edge state at interface between topological band insulator (left) and Mott insulator (right). Shown is the partially integrated density of states $-\beta g_{11}(y, \beta/2)$ of orbital $\alpha = 1$ as a function of layer index. The embedding region consists of 21 layers: 6 layers at $U_L = 2$ and 15 layers in the range $U_R = 13 \dots 15$. Outside the embedding range, bulk behavior is assumed. The location of the edge state is seen to be a sensitive function of the Coulomb energy in the Mott insulator. The maximum value $-\beta g_{11}(\beta/2) \approx 0.33$ is associated with the Kondo peak. (b) Amplitude of the edge state as a function of layer index at $U_R = 12.75$ for increasing numbers of iterations in the self-consistency procedure. The maximum due to the Kondo peak is seen to shift toward the right-hand side of the embedding region. The solid vertical line locates the phase boundary between topological and Mott insulating phases, with both having the same Coulomb repulsion $U = 12.75$, at the 160th DMFT iteration.

at the free surface (see Fig. 3) with the corresponding value (≈ 0.18) in the surface layer for $U_L = 2$ (Fig. 7(a)). Thus, the Kondo peak in the Mott insulator gives rise, via the single-particle hopping across the interface, to a low-energy spectral feature at the surface of the topological band insulator. Note that this feature is also present for $U_L = 0$. It is therefore not induced by the small local self-energy in the band insulator, but by the large self-energy in the neighboring layer exhibiting the Kondo peak. This mechanism may therefore be viewed as a 'reverse proximity effect', in contrast to the usual one, in which the metal states induce the Kondo peak in the Mott insulator. This kind of 'feedback' effect occurs also

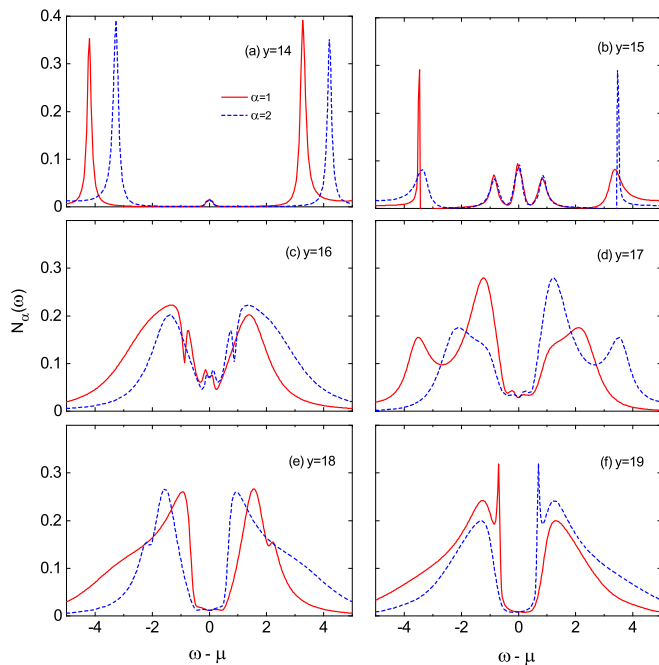


FIG. 8: (Color online) (a) Interacting DOS, $N_\alpha(\omega)$, at interface between topological band insulator ($U_L = 2$) and Mott insulator ($U_R = 15$). Solid (red) curves: orbital $\alpha = 1$, dashed (blue) curves: orbital $\alpha = 2$. Panels (a) and (b) correspond to two surface layers on the right of the interface ($y = 14, 15$ in Fig. 7), panels (c) to (f) to four surface layers on the left of the interface ($y = 16 \dots 19$). These spectra are obtained by extrapolating the lattice Green's function to $\omega + i\gamma$ with a small imaginary energy $\gamma = 0.05$ via the routine *ratint*. The central spectral feature in panel (b) corresponds to the Kondo peak induced in the Mott insulator via the usual proximity effect due to the metallic edge state, while in panel (c) the low-energy feature is induced in the surface layer of the topological insulator via a reverse proximity effect caused by the Kondo peak.

at interfaces between ordinary metals and Mott insulators (see, for instance, the small peak for $x = 0$ in Fig. 1 of Ref. 20). In the latter case, however, this effect is very small because of the dominant metallic DOS. In the present heterostructure, this effect is much more pronounced because of the minimum of the density of states of the edge state in the surface layer of the topological band insulator.

So far we have discussed the formation of the Kondo peak for $U_L = 2$ and $U_R = 15$. Returning to Fig. 7(a), we point out that, when the Coulomb energy U_R in the right-hand system is lowered, the maximum of the edge state shifts away from the interface toward the interior of the Mott insulator. Evidently, due to the proximity of the topological band insulator, the topological band insulating phase is more stable in the surface region of the Mott insulator, so that the effective boundary between the topological and Mott phases moves away from the physical interface. From a numerical point of view, one

observes that the self-energy and cluster parameters of the boundary layers are converted from those characteristic of the Mott insulator phase to those characteristic of the topological insulator phase with increasing iterations, in a layer-by-layer fashion, starting from the first boundary layer, toward the interior of the Mott insulator, until no further phase conversion of layers takes place.

Note that for the lowest two Coulomb energies shown in Fig. 7(a) ($U_R = 13.0$ and $U_R = 13.2$), the Mott insulator is within the bulk coexistence region ($U_{c2} \approx 13.4$, see Fig. 2), so that the actual phase depends sensitively on the properties near the interface. For $U_R = 13.2$, the bulk Mott insulator phase is more stable than the bulk topological insulator phase, so that the DOS profile shown in Fig. 7(a) does not shift any more with further iterations. On the other hand, $U_R = 13.0$ seems to be very close to U_b , so that one needs hundreds of iterations to reach the DOS profile in Fig. 7(a). It is to be noted that to ensure the persistence of the edge state at these Coulomb energies, the bulk phase in the asymptotic region on the right-hand side is assumed to be Mott insulating. As discussed in the previous subsection, if instead both constituents of the heterostructure are topological band insulators, the edge state disappears.

To illustrate this delicate balance between topological and Mott insulating solutions in the interface region, we show in Fig. 7(b) the edge state for $U_L = 2$ and $U_R = 12.75$. Beyond the 15 surface layers of the right-hand system, bulk Mott insulating behavior is assumed. In addition, these 15 layers are initially assumed to be in the Mott insulating phase. With increasing number of iterations, the peak of the edge state is seen to shift toward the right side of the embedded region. Apparently, at $U_R = 12.75$, the bulk topological insulator phase is more stable than the bulk Mott insulator phase, so that the conversion of layers from the Mott phase to topological phase does not stop until all layers in the embedded region are converted. In other words, for this value of U_R , one cannot find a stable Mott solution of the DMFT equation in contrast to the cases with larger U_R shown in panel (a). The marked increase of spectral weight between layers 15 and 16 reflects the fact the nominal boundary of the heterostructure now comprises neighboring topological insulating phases for different values of U (see Fig. 6). Accordingly, the shape of the 'buried' edge state within the right-hand system approaches that at the interface between systems with identical Coulomb energies in the coexistence range, but with topological band insulating and Mott insulating phases present on either side.

The edge state in such a case is shown in Fig. 9 for $U_L = U_R = 13$, where bulk Mott insulating (bulk topological band insulating) behavior is enforced on the right (left) side of the embedding region, respectively. The asymptotic value of $-\beta g_{11}(y, \beta/2)$ on the right-hand side is very small because of the large size of the Mott gap. For the same reason, the decay of the edge state in the Mott insulator is more rapid than within the band insu-

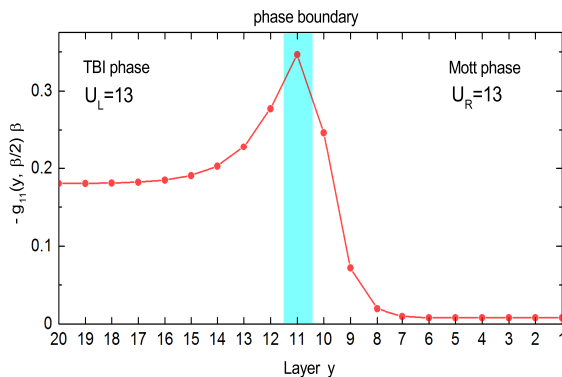


FIG. 9: (Color online) Edge state at interface between topological band insulator and Mott insulator in the coexistence region with $U_L = U_R = 13$. The Mott gap at this Coulomb energy is much larger than the topological band gap. Thus, the asymptotic value of $-\beta g_{11}(y, \beta/2)$ on the right-hand side is much lower than on the left-hand side, and the decay of the edge state within the Mott insulator is more rapid. The vertical bar denotes the Kondo peak in the surface layer of the Mott insulator at the effective boundary with the topological band insulator.

lator. The spatial distribution of this edge state is very similar to the one in Fig. 7 deep within the nominal Mott insulator. As stated above, since $U_L = U_R = 13$ is very close to U_b at $T = 0.01$, the bulk topological insulator on the left-hand side and the bulk Mott insulator on the right-hand side have nearly the same stability. Therefore, the DOS profile in Fig. 9 does not move with additional DMFT iterations.

Evidently, the phenomenon observed in Fig. 7 is a proximity effect, where the band insulating properties on one side of the interface are induced up to a certain depth on the other side, for instance, via the penetration of the edge state wave function across the boundary layer, although asymptotically this side is a Mott insulator. The boundary between band and Mott insulating phases then does not coincide with the nominal interface.

The results discussed above suggest that the embedding scheme might be useful for the study of the relative stability of coexisting phases in DMFT calculations. Let us assume $U_L = U_R = U$ lies in the coexistence domain, with band insulating (Mott insulating) properties enforced on the left (right) side of the embedded region. As long as $U_{c1}(T) < U < U_b(T)$, the topological band insulating solution is more stable, so that the edge state will be located at the right boundary of the embedded region. Conversely, if $U_b(T) < U < U_{c2}(T)$, the Mott phase is more stable, so that the edge state shifts toward the left boundary.

IV. SUMMARY

The edge state at the interface between topological band and Mott insulators has been investigated within inhomogeneous DMFT. The generalized Bernevig-Hughes-Zhang two-band model is used to describe the interplay between interorbital hybridization and local Coulomb energy. The electronic properties in the vicinity of the interface are treated self-consistently by making use of the embedding scheme, where the effect of the asymptotic semi-infinite bulk materials is described in terms of complex local potentials. The finite-temperature exact diagonalization method is employed to evaluate the on-site many-body interactions.

The main result of this work is the observation that, close to the critical Coulomb energy of the correlated topological insulator, the edge state is expelled from the interface toward the interior of the Mott insulator. Thus, as a result of the proximity with the topological band insulator, the Mott insulating phase within a certain depth is converted to a topological band insulating phase, where the width of the conversion region depends on the local Coulomb energy within the Mott insulator. With increasing Coulomb energy, the Mott gap widens and the topological edge state is pushed again toward the interface. Its decay within the Mott insulator then becomes more rapid. At Coulomb energies below the Mott transition, the edge state ceases to exist since in this case the interface corresponds to that between two weakly and moderately correlated topological band insulators.

The origin of the interface-induced conversion from Mott insulating to band insulating behavior is the coexistence region associated with the first-order nature of the Mott transition. Depending on the temperature of the sample, either the Mott insulating or the band insulating solution is more stable at a given value of the local Coulomb energy. These results suggest that the embedding method might be useful to determine the relative stability of Mott and band insulating phases in DMFT calculations. In addition, the conversion between Mott and band insulating phases might be observed experimentally in alloy heterostructures in which the existence of these phases can be tuned continuously by varying the material parameters.

We have also shown that the normal proximity effect, where a Kondo peak in a Mott insulator is induced via neighboring metallic states, gives rise to a reverse proximity effect, where the Kondo peak leads to an enhanced density of states at the surface of the neighboring metal.

Acknowledgments

The work of H. I. was supported by JSPS KAKENHI (No. 24540328). H.I. thanks the Alexander von Humboldt foundation for support. Part of the computations were carried out using the Jülich Juropa Supercomputer. A. L. thanks Theo Costi for useful discussions.

-
- ¹ For a review, see: M. Hohenadler and F. F. Assaad, J. Phys. Condens. Mat. **25**, 143201 (2013).
- ² A. Shitade, H. Katsura, J. Kunes, X.-L. Qi, S. C. Zhang, and N. Nagaosa, Phys. Rev. Lett. **102**, 256403 (2009).
- ³ D. A. Pesin and L. Balents, Nature Phys. **6**, 376 (2010).
- ⁴ T. Yoshida, S. Fujimoto, and N. Kawakami, Phys. Rev. B **85**, 125113 (2012).
- ⁵ B. A. Bernevig, T. L. Hughes, and S. C. Zhang, Science, **314**, 1757 (2006).
- ⁶ M. Z. Hasan and C. L. Kane, Rev. Mod. Phys. **82**, 3045 (2010).
- ⁷ X. L. Qi and S. C. Zhang, Rev. Mod. Phys. **83**, 1057 (2011).
- ⁸ C. Wu, B. A. Bernevig, and S. C. Zhang, Phys. Rev. Lett. **96**, 106401 (2006).
- ⁹ C. Xu and J. E. Moore, Phys. Rev. B **73**, 045322 (2006).
- ¹⁰ Y. Yamaji and M. Imada, Phys. Rev. B **83**, 205122 (2011).
- ¹¹ J. A. Hutasoit and T. D. Stanescu, Phys. Rev. B **84**, 085103 (2011).
- ¹² B.-J. Yang, M. S. Bahramy, and N. Nagaosa, Nature Commun. **4**, 1524 (2013).
- ¹³ X. Wang, G. Bian, T. Miller, and T.-C. Chiang, Phys. Rev. B **87**, 235113 (2013).
- ¹⁴ S. Ueda, N. Kawakami, and M. Sgrist, Phys. Rev. B **87**, 161108(R) (2013).
- ¹⁵ T. Rauch, M. Flieger, J. Henk, and I. Mertig, Phys. Rev. B **88**, 245120 (2013).
- ¹⁶ S. Essert, V. Krueckl, and K. Richter, arXiv:1402.1095 (2014).
- ¹⁷ A. Georges, G. Kotliar, W. Krauth, and M. J. Rozenberg, Rev. Mod. Phys. **68**, 13 (1996).
- ¹⁸ M. Potthoff and W. Nolting, Phys. Rev. B **59**, 2549 (1999).
- ¹⁹ S. Okamoto and A. J. Millis, Nature (London) **428**, 630 (2004).
- ²⁰ R. W. Helmes, T. A. Costi, and A. Rosch, Phys. Rev. Lett. **101**, 066802 (2008).
- ²¹ A. Koga, T. Higashiyama, K. Inaba, S. Suga, and N. Kawakami, Phys. Rev. A **79**, 013607 (2009).
- ²² H. Ishida and A. Liebsch, Phys. Rev. B **79**, 045130 (2009); *ibid.* **85**, 045112 (2012).
- ²³ E. V. Gorelik, I. Titvinidze, W. Hofstetter, M. Snoek, and N. Blümer, Phys. Rev. Lett. **79**, 065301 (2010).
- ²⁴ M. Caffarel and W. Krauth, Phys. Rev. Lett. **72**, 1545 (1994).
- ²⁵ C. A. Perroni, H. Ishida, and A. Liebsch, Phys. Rev. B **75**, 045125 (2007).
- ²⁶ A. Liebsch and H. Ishida, J. Phys.: Condens. Matter **24** 053201 (2012).
- ²⁷ J. E. Inglesfield, Comput. Phys. Commun. **137**, 89 (2001).
- ²⁸ Y. Tada, R. Peters, M. Oshikawa, A. Koga, N. Kawakami, and S. Fujimoto, Phys. Rev. B **85**, 165138 (2012).
- ²⁹ H. Zenia, J. K. Freericks, H. R. Krishnamurthy, and T. Pruschke, Phys. Rev. Lett. **103**, 116402 (2009).
- ³⁰ G. Borghi, M. Fabrizio, and E. Tosatti, Phys. Rev. B **81**, 115134 (2010).
- ³¹ M. Dzero, K. Sun, V. Galitski, and P. Coleman, Phys. Rev. Lett. **104**, 106408 (2010); M. Dzero, K. Sun, P. Coleman, and V. Galitski, Phys. Rev. B **85**, 045130 (2012).
- ³² J. Werner and F.F. Assaad, Phys. Rev. B **89**, 245119 (2014).
- ³³ M. Sentef, J. Kunes, Ph. Werner, and A. P. Kampf, Phys. Rev. B **80**, 155116 (2009)
- ³⁴ F. Grandi, F. Manghi, O. Corradini, C. M. Bertoni, and A. Bonini, arXiv:1404.1287.